Robotica (2008) volume 26, pp. 791–802. © 2008 Cambridge University Press
doi:10.1017/S0263574708004384 Printed in the United Kingdom

Wrench capabilities of planar parallel manipulators. Part I: Wrench polytopes and performance indices

Flavio Firmani†, Alp Zibil†, Scott B. Nokleby‡ and Ron P. Podhorodeski†*

†*Robotics and Mechanisms Laboratory, Department of Mechanical Engineering, University of Victoria, P.O. Box 3055, Victoria, B. C, V8W 3P6, Canada*
‡*Faculty of Engineering and Applied Science, University of Ontario Institute of Technology, 2000 Simcoe Street North, Oshawa, Ontario, L1H 7K4, Canada*

(Received in Final Form: February 2, 2008. First published online: April 15, 2008)

SUMMARY
This paper is organized in two parts. In Part I, the wrench polytope concept is presented and wrench performance indices are introduced for planar parallel manipulators (PPMs). In Part II, the concept of wrench capabilities is extended to redundant manipulators and the wrench workspace of different PPMs is analyzed. The end-effector of a PPM is subject to the interaction of forces and moments. Wrench capabilities represent the maximum forces and moments that can be applied or sustained by the manipulator. The wrench capabilities of PPMs are determined by a linear mapping of the actuator output capabilities from the joint space to the task space. The analysis is based upon properly adjusting the actuator outputs to their extreme capabilities. The linear mapping results in a wrench polytope. It is shown that for non-redundant PPMs, one actuator output capability constrains the maximum wrench that can be applied (or sustained) with a plane in the wrench space yielding a facet of the polytope. Herein, the determination of wrench performance indices is presented without the expensive task of generating polytopes. Six study cases are presented and performance indices are derived for each study case.

KEYWORDS: force/moment capabilities; planar parallel manipulators; polytopes; wrench performance indices; screw theory.

1. Introduction

1.1. Instantaneous twist and wrench capabilities

The instantaneous twist and wrench capability analyses are essential for the design and performance evaluation of serial and parallel manipulators. An instantaneous twist is a screw quantity that contains both angular and translational velocities of the end-effector; whereas, a wrench is a screw quantity that contains the forces and moments acting on the end-effector. For a given pose, the end-effector is required to move with a desired twist and to sustain (or apply) a specified wrench. Thus, the information of the joint velocities and joint torques that will produce such conditions could be investigated. These studies are referred to as the inverse velocity and static force problems and are described in Appendix A. In addition, an extended problem can be formulated as the analysis of the maximum twist or wrench that the end-effector can perform in the twist or wrench spaces, respectively. The knowledge of maximum twist and wrench capabilities is an important tool for achieving the optimum design of manipulators. In Part I of this paper, the wrench capabilities are analyzed for a specific manipulator pose and wrench performance indices are derived. In Part II, this analysis is extended to the overall workspace of the manipulator and is represented with plots of force and moment capabilities. By being able to graphically visualize the twist and wrench capabilities, comparisons between different design parameters, such as the actuator torque capabilities and the dimensions of the links, can be explored. Also, the performance of an existing manipulator can be improved by identifying the optimal capabilities based on the configuration of the branches and the pose of the end-effector.

This work focuses on the wrench capabilities of planar parallel manipulators (PPMs), the geometric interpretation of their wrench polytopes, the derivation of wrench performance indices, and how the inclusion of redundancy affects the performance of PPMs.

The wrench capability analysis of a manipulator depends on its design, posture, and actuator torque capabilities. To date, the study of wrench capabilities has been approached in three different forms: constrained optimization, wrench ellipsoids, and wrench polytopes.

1.2. Constrained optimization

Early works on wrench capabilities dealt with the problem of force distribution of two serial manipulators handling a common payload. Zheng and Luh[1] developed an algorithm that incorporates maximum torque capabilities. Two analyses were presented. The first analysis ensured that the forces applied by the branches were in the same direction as the required force. The second analysis ensured that the load

* Corresponding author. E-mail: podhoro@me.uvic.ca

was evenly distributed between the two serial arms. Kumar and Waldron[2] investigated force distribution in redundantly-actuated closed-loop kinematic chains and concluded that there would be zero internal forces using the Moore–Penrose pseudo-inverse solution. Tao and Luh[3] developed an algorithm that determines the minimum torque required to sustain a common load between two joint-redundant cooperating manipulators. Nahon and Angeles[4] described the problem of a hand grasping an object as a redundantly-actuated kinematic chain. The problem was formulated with both equality and inequality constraints and the torques were found by minimizing the internal forces in the system using Quadratic Programming (QP). Kwon and Lee[5] modelled the joint torque limits and the exerting force of each cooperating manipulator as quadratic constraints. This allowed them to implement the dual method, which is based on combining nonlinear programming with QP, resulting in a more efficient algorithm than the one proposed by Nahon and Angeles.[4] Buttolo and Hannaford[6] analyzed the force capabilities of a redundant PPM. Torques were optimized using the ∞-norm resulting in higher force capabilities when compared to the pseudo-inverse solution. Nokleby *et al.*[7] developed a methodology to optimize the force capabilities of redundantly-actuated PPMs using an n-norm, for large values of n, and a scaling factor. Garg *et al.*[8] implemented this approach to spatial parallel manipulators.

The wrench of a PPM is referred to as the two components of the forces on the plane (f_x and f_y) and the moment normal to the plane (m_z). Finding the wrench capabilities of a planar manipulator as a constrained optimization problem is subject to the forward static force equation and the actuator output capabilities, i.e.,

$$\text{maximize } f \quad \text{or} \quad \text{maximize } m_z \tag{1}$$

subject to:

$$[\$'\mathbf{D}]\boldsymbol{\tau} = \mathbf{F} \tag{2}$$
$$\tau_{i_{\min}} \leq \tau_i \leq \tau_{i_{\max}}$$

where $[\$'\mathbf{D}]$ is a known numerical matrix defined by the geometry and the pose of the manipulator (details of its formulation can be found in Appendix A). This matrix is also referred to in the literature as $[\mathbf{J}]^{-\mathrm{T}}$, with $[\mathbf{J}]$ being the kinematic Jacobian matrix. The output wrench for the planar case is denoted as $\mathbf{F} = \{f_x, f_y; m_z\}^{\mathrm{T}} = \{f\cos\alpha, f\sin\alpha; m_z\}^{\mathrm{T}}$, with f and α defining the magnitude and direction of the vector force, and $\boldsymbol{\tau}$ is the vector of actuator torques. The actuator torque of the i^{th} branch is defined as τ_i; this torque is bounded by the actuator output capabilities, i.e., $\tau_{i_{\max}}$ and $\tau_{i_{\min}}$, referred to as extremes. In general, a revolute actuator provides the same torque in both directions, i.e., $|\tau_{i_{\min}}| = |\tau_{i_{\max}}|$.

The optimization approach is usually computationally expensive and may not yield the correct solution because the optimization algorithm may encounter a local minimum rather than the desired global minimum due to the non-linear nature of the problem.

1.3. Wrench ellipsoid

For serial manipulators, Yoshikawa[9,10] introduced manipulability measurements which quantify the twist and wrench capabilities of the end-effector. Let the actuator torque vector be bounded by a unit hypersphere in the joint force space, i.e.,

$$\boldsymbol{\tau}^{\mathrm{T}}\boldsymbol{\tau} \leq 1 \tag{3}$$

Then, since

$$\boldsymbol{\tau} = [\mathbf{J}]^{\mathrm{T}}\mathbf{F}$$

a mapping of the task wrench space is derived as follows

$$\mathbf{F}^{\mathrm{T}}[\mathbf{J}][\mathbf{J}]^{\mathrm{T}}\mathbf{F} \leq \mathbf{1} \tag{4}$$

The above equation is the representation of the manipulating-force (wrench) ellipsoid. A similar analysis can be carried out to find the manipulability (twist) ellipsoid.

Assuming the singular value decomposition (SVD) of $[\mathbf{J}]$ yields

$$[\mathbf{J}] = [\mathbf{U}][\Sigma][\mathbf{V}]^{\mathrm{T}} = [\mathbf{U}]\begin{bmatrix}\mathbf{S} & \mathbf{0}\\ \mathbf{0} & \mathbf{0}\end{bmatrix}[\mathbf{V}]^{\mathrm{T}} \tag{5}$$

where $[\mathbf{U}] \in \Re^{n\times n}$ and $[\mathbf{V}] \in \Re^{m\times m}$ are orthogonal matrices, $[\Sigma] \in \Re^{n\times m}$, and $[\mathbf{S}] = diag(\sigma_1, \sigma_2, \ldots, \sigma_n)$ is a diagonal matrix that contains the singular values in decreasing magnitude or numerical order, i.e., $\sigma_1 \geq \sigma_2 \geq \cdots \geq \sigma_n \geq 0$. The principal axes of the wrench ellipsoid are given by $\mathbf{u}_1/\sigma_1$, $\mathbf{u}_2/\sigma_2$, ..., and $\mathbf{u}_n/\sigma_n$; where $\mathbf{u}_i$, the i^{th} column of matrix $[\mathbf{U}]$, and $1/\sigma_i$ define the direction and magnitude of the i^{th} principal axis, respectively.

For cooperating manipulators, Chiacchio *et al.*[11] presented a complete analysis of wrench ellipsoids for multiple-arm systems, which involves external and internal forces. Lee and Kim[12] (velocity problem) and Chiacchio *et al.*[13,14] (static force problem) proposed to normalize the joint space variables (joint velocities and joint torques, respectively) when the actuators do not produce the same output. As a result, the resulting ellipsoid is defined as the pre-image of the unit sphere in the scaled joint variable space.

The concept of manipulability has also been extended to manipulator dynamics, where the acceleration ellipsoid has been investigated.[15,16]

Nevertheless, the ellipsoid approach presents an important drawback due to an improper use of the Euclidean metric in the wrench and twist screw spaces.[17] Any change of the scale, physical units, or reference frame will affect quantities derived from the Jacobian matrix. Doty *et al.*[18] showed that even though Eq. (4) has consistent units, the characterizing matrix $[\mathbf{J}][\mathbf{J}]^{\mathrm{T}}$ is ill defined because it is not invariant to the selection of origin or scaling. Therefore, any quantity resulting from the orthogonal complements of Eq. (5) will produce incongruent results. Doty *et al.*[18] proposed a manipulability measure that is invariant to reference frame transformations and scaling. Melchiorri[19] presented some examples where the implementation of the wrench ellipsoid approach fails when applied to cooperating manipulators with less than 6-DOF (degree-of-freedom) per cooperating branch. Bicchi *et al.* addressed the twist ellipsoid problem[20]

https://doi.org/10.1017/S0263574708004384 Published online by Cambridge University Press

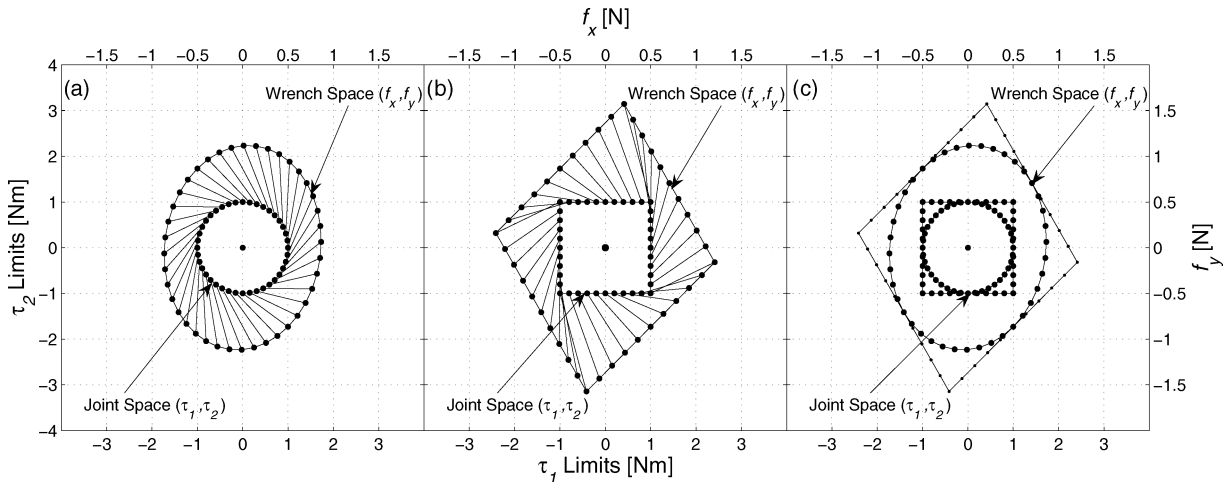

Fig. 1. Mapping of ellipsoids and polytopes from the joint space to the task space.

and the wrench ellipsoid problem[21] to general cooperating manipulators with an arbitrary number of joints per branch.

1.4. Wrench polytope

The feasible region in $\Re^m$ of joint velocities/torques may be modeled with either the Euclidean norm yielding a hypersphere using the ellipsoid approach or with the ∞-norm yielding a hypercube using the polytope approach. Kokkinis and Paden[22] introduced the concept of twist and wrench convex polytopes. The analysis was applied to a single serial manipulator and to two cooperating manipulators, and led to an accurate representation of the actuator constraints. Polytopes are an exact representation of the joint capabilities in the task space ($\Re^n$). Polytopes are generated by mapping the range of joint velocities/torques (hypercubes, polytopes themselves) to the twist/wrench space by means of the Jacobian matrix. Thus, a polytope results from a linear transformation from a hypercube, while an ellipsoid results from the same linear transformation of a hypersphere.

The volume defined by either the ellipsoid or the polytope represents feasible twists or wrenches. This is, a vector from the origin of the twist/wrench space to the surface of the ellipsoid or polytope represents the maximum twist/wrench that can be reached. Nevertheless, the difference between the two approaches is that the hypersphere is fully inscribed within the hypercube; consequently, the ellipsoid is fully inscribed within the polytope. Thus, the region of the polytope that is not contained by the ellipsoid may be seen as unreachable. Therefore, if the objective is to maximize the twist or wrench capabilities, the model of joint velocities and torque limits is better represented by a hypercube (polytope approach) than by a hypersphere (ellipsoid approach).

A comparison between the ellipsoid and polytope approaches is shown in Fig. 1. Assume a manipulator with two actuated revolute joints whose extreme capabilities are $\tau_{i_{ext}} = \pm 1$ Nm, for $i = 1, 2$. Figure 1a shows the generation of an ellipse (in general, an ellipsoid) as a result of mapping a circle (hypersphere). Figure 1b shows the generation of a polygon (polytope) as a result of mapping a square (hypercube). Each plot contains two coordinate systems. The inner circle of Fig. 1a and the inner square of Fig. 1b describe the torque limits in the torque space (bottom and left axes); whereas, the outer ellipse and polygon describe the wrench capabilities in the wrench space (top and right axes). The lines that connect the inner to the outer shapes illustrate the linear transformation. Note how the edges and vertices of the square and polygon correspond in both spaces.

The areas comprised by these geometrical shapes represent the feasible capabilities in their corresponding spaces. The square is an exact representation of the torque capabilities; while, the circle is an approximation. For example, the upper-right vertex of the square is $\tau_1 = \tau_2 = 1$ [Nm]; although this torque combination is feasible, the circle does not include it. Thus, modeling the torque capabilities as a square is better than as a circle. Figure 1c shows how the circle and ellipse are inscribed within the square and polygon, respectively. It is important to mention that the principal axes of the ellipse are directed toward the vertices of the polygon.

A polytope is a convex region, i.e., any two points inside the polytope can be connected by a line that completely fits inside the polytope. An n-dimensional convex polytope is bounded by $(n-1)$-dimensional facets or hyperplanes, e.g., linear edges in $\Re^2$ bounding a polygon or planar facets in $\Re^3$ bounding a polyhedron. Finding the vertices of the polytope can be computationally expensive. Bicchi *et al.*[20] presented an algorithm that involves slack variables that transform the inequality constraints of the actuator limits into equality constraints. Lee[23] proposed a method for determining the vertices of twist polytopes using vector algebra. Hwang *et al.*[24] developed an algorithm that generates the twist polytope of redundant serial manipulators.

Further studies on kinetostatic polytopes have been made. Chiacchio *et al.*[13,14] analyzed the wrench polytopes of redundant serial manipulators. Finotello *et al.*[25] introduced two sets of indices that can be implemented to twist and wrench polytopes: the maximum isotropic value (MIV) and the maximum available value (MAV). These indices will be discussed in detail in Section 3. For 6-DOF manipulators, Finotello *et al.*[25] proposed to analyze these indices with force and moment as separate entities.

Gallina[26] analyzed the manipulability of a 3-DOF wire driven planar haptic device using polytopes. Lee and Shim[27] expanded the concept to dynamic manipulability of multiple

https://doi.org/10.1017/S0263574708004384 Published online by Cambridge University Press

cooperating manipulators resulting in acceleration polytopes. Krut *et al.*[28] analyzed twist ellipsoids and polytopes in redundant parallel manipulators and established performance indices. They showed that there is another ellipsoid, besides the one derived with SVD, which is larger in volume and is fully inscribed within the polytope. Krut *et al.*[29] also studied force performance indices of redundant parallel manipulators and determined the isotropic wrench workspaces of planar wire-driven manipulators with multiple actuated limbs.

2. Wrench Polytope Analysis

The differences between the ellipsoid and the polytope approaches can be summarized with two arguments. First, a polytope represents the exact mapping of the joint capabilities in the wrench or twist space, while the ellipsoid approach only provides an approximation of such mapping. Furthermore, the ellipsoid approach is more susceptible to errors when implemented on redundantly actuated parallel manipulators, as shown by Krut *et al.*[28] Second, the ellipsoid approach can be implemented easily and the required computation is immediate, while the polytope approach may be considered less efficient because it requires two steps: determination of potential vertices and the construction of the polytope. The vertices are formed from a set of potential vertices which can be internal or external points, the latter being the vertices of the polytope.

Most of the papers that have dealt with wrench or twist polytopes have usually attempted to improve the computational efficiency of the construction of convex polytopes. In this paper, it is shown that the determination of wrench performance indices using the polytope approach is actually very efficient because they can be determined with the knowledge of potential vertices, and no construction of the polytope is required.

Let n be the DOF of the task space coordinates and m be the number of actuated joints. The i^{th} joint torque variable, which is bounded by $\tau_{i_{\min}}$ and $\tau_{i_{\max}}$, can be represented in the joint torque space as two parallel planes in $\Re^m$. With m joints, there are $2m$ planes or m pairs of parallel planes. The combination of all the parallel planes that constrain the joint torque limits form an m-dimensional parallelepiped. If all the torque limits were equal, the m-dimensional parallelepiped would result in a hypercube. If the magnitude of the extreme torques were equal, the parallelepiped would be centro-symmetric; otherwise, skewed.

For example, assume three actuators, i.e., $m = 3$. Each actuator torque defines an axis in $\Re^3$. The extremes of each torque constrain the torque space with a pair of parallel planes. The feasible region of the actuator torques is bounded by the three pairs of parallel planes, i.e., a three-dimensional parallelepiped. If the torque magnitudes and extremes were equal a centro-symmetric cube would result.

The vertices are generated with the intersection of m extreme torque planes, one for each actuator. The total combination of m intersecting extreme torque planes yields the number of vertices. In general, vertices are formed as a combination of the extreme values, i.e.,

$$v_i = \begin{bmatrix} \tau_{1_{ext}} & \tau_{2_{ext}} & \dots & \tau_{m_{ext}} \end{bmatrix}^{\mathrm{T}} \tag{6}$$

where $\tau_{i_{ext}}$ denotes the extreme capabilities of the i^{th} actuator, i.e., $\tau_{i_{\min}}$ or $\tau_{i_{\max}}$. Thus, the total number of vertices in the m-dimensional parallelepiped[14] is $v_{T_m} = 2^m$. For the case when $m = 3$, there are $v_{T_m} = 2^3 = 8$ vertices.

A linear transformation, such as the equation of the forward static force in Eq. (27), maps vector $\boldsymbol{\tau}$ from $\Re^m$ (joint torque space) to $\Re^n$ (wrench space). Rockafellar[30] studied the properties of convex polyhedral sets. From his analysis, the following relationship is held through a linear transformation: Let C be the m-dimensional parallelepiped (a convex set) and $[\$'\mathbf{D}]$ be the linear transformation from $\Re^m$ to $\Re^n$. Then the resulting transformation $[\$'\mathbf{D}]C$ leads to another convex polyhedral set in $\Re^n$ and it contains a finite number of facets.

Visvanathan and Milor[31] investigated the problems in analog integrated circuits while accounting for the tolerance variations of the principal process parameters. The problem involved the mapping of a parallelepiped under a linear transformation. Their mathematical formulation is similar to the one used for analyzing wrench capabilities in this work.

Assume a parallelepiped in $\Re^m$ centered at the origin of the torque space and let the coordinates of its vertices be v_i, $i = 1, \dots, 2^m$. Under a matrix transformation $[\$'\mathbf{D}]$ from $\Re^m$ to $\Re^n$, the m-dimensional parallelepiped becomes a centro-symmetric[31] polytope P. Thus, P can be completely characterized by mapping all the vertices and enclosing them in a convex hull, i.e.,

$$P = \text{convh}\{[\$'\mathbf{D}]v_i,\ i = 1, \dots, 2^m\} \tag{7}$$

where "convh" denotes a convex hull operator which encloses all the extreme points (or vertices of the polytope) forming the feasible region of the torque space in the wrench space. A closed bounded convex set is the convex hull of its extreme points.[30]

The total number of vertices in the polytope, v_{T_n}, will depend on the dimension of the two spaces. If $n = m$, the number of vertices in the polytope equals the number of vertices in the m-dimensional parallelepiped, i.e., $v_{T_n} = v_{T_m}$. This similarity is given by the linear transformation between the two spaces. Thus, vertices, edges, and facets of the polytope are the corresponding image of the vertices, edges, and facets of the m-dimensional parallelepiped, respectively, i.e.,

$$p_i = [\$'\mathbf{D}]v_i \tag{8}$$

for $i = 1, \dots, 2^m$, where p_i and v_i are the vertices of the polytope and parallelepiped, respectively.

If $n < m$, as in a redundantly actuated manipulator, then $v_{T_n} < v_{T_m}$. In this case, the vertices of the polytope are formed with the mapping of some of the vertices of the m-dimensional parallelepiped, i.e.,

$$p_j \subset [\$'\mathbf{D}]v_i \tag{9}$$

with $j < i$. The points that do not form the vertices of the polytope are internal points in P. The characteristics of these internal points are considered in Part II of this work.

The generation of a polytope through a convex hull has been studied thoroughly in the field of computational

https://doi.org/10.1017/S0263574708004384 Published online by Cambridge University Press

geometry and the goal has been to make a more efficient algorithm. Chand and Kapur[32] proposed the so-called *gift wrapping* algorithm, where the facets of a polytope are found by determining the angles between one vertex and the rest of the points. The minimum and maximum angles correspond to the hyperplanes passing through that point. Visvanathan and Milor[31] proposed an algorithm that searches in the directions that are orthogonal to each of the known hyperplanes. New vertices and hyperplanes are formed and the process is repeated. Hwang *et al.*[24] developed a recursive algorithm that removes all the internal points when first encountered. Hwang *et al.* also showed that even though the number of potential vertices grows exponentially (2^m), the number of external points increases linearly. The scope of this paper is not to develop a new algorithm for determining polytope facets, although some of the concepts that will be described in this work may be used to generate an even more efficient algorithm.

3. Wrench Performance

3.1. Methodology

In order to analyze the wrench capabilities of PPMs, Zibil *et al.*[33] proposed four study cases and elaborated a methodology to explicitly identify wrench capabilities. The methodology was based upon properly adjusting the actuator outputs to their extreme capabilities. Herein, the previously developed method is explained, the formulation is improved, and two additional study cases are presented. The wrench performance indices that can be derived from each study case are also presented. In addition, a focal point of this work is to present a geometric interpretation of the wrench polytopes and the wrench performance indices for both non-redundant (Part I) and redundant (Part II) PPMs.

In this section six studies of wrench capabilities will be presented and applied to the 3-RRR PPM. The characteristics of this manipulator are described in Appendix B. The mobile platform will be located at the center of the workspace. The force coordinate system is coincident with the center of the mobile platform and with a constant orientation of zero degrees.

Since $n = m$ for the 3-RRR PPM, the forward static force equation is

$$\mathbf{F} = [\$'\mathbf{D}]\boldsymbol{\tau}$$

$$\begin{bmatrix} f_x \\ f_y \\ m_z \end{bmatrix} = \begin{bmatrix} sd_{1,1} & sd_{1,2} & sd_{1,3} \\ sd_{2,1} & sd_{2,2} & sd_{2,3} \\ sd_{3,1} & sd_{3,2} & sd_{3,3} \end{bmatrix} \begin{bmatrix} \tau_1 \\ \tau_2 \\ \tau_3 \end{bmatrix} \tag{10}$$

while the vertices of the polytope are determined with Eq. (8), i.e.,

$$p_i = [\$'\mathbf{D}]v_i \qquad \text{for } i = 1, 2, 3.$$

$$\begin{bmatrix} f_x \\ f_y \\ m_z \end{bmatrix} = \begin{bmatrix} sd_{1,1} & sd_{1,2} & sd_{1,3} \\ sd_{2,1} & sd_{2,2} & sd_{2,3} \\ sd_{3,1} & sd_{3,2} & sd_{3,3} \end{bmatrix} \begin{bmatrix} \tau_{1_{ext}} \\ \tau_{2_{ext}} \\ \tau_{3_{ext}} \end{bmatrix} \tag{11}$$

For a PPM, the resulting polytope described in $\Re^3$ has the following characteristics:

(i) Any point outside the polytope is a wrench that cannot be applied or sustained;
(ii) Any point inside the polytope is achieved with actuators that are not working at their extreme capabilities;
(iii) Any point on a facet of the polytope has one actuator working at an extreme capability;
(iv) Any point on an edge of the polytope has two actuators working at their extremes;
(v) Any vertex of the polytope has all three actuators working at their extremes.

In the following study cases, performance indices are identified. These indices represent points of the polytope. To determine a particular performance index, Eq. (10) is rearranged as a linear system of three equations of the form $\mathbf{Ax} = \mathbf{b}$; where $\mathbf{x}$ is a vector that contains all of the unknown variables, either wrench or torque space coordinates, $\mathbf{A}$ is a coefficient matrix, and $\mathbf{b}$ is a vector that contains the torques that are set to their extreme capabilities. For different study cases, Zibil *et al.*[33] presented a comprehensive explanation of the arrangements of $\mathbf{Ax} = \mathbf{b}$. An important improvement of the new approach is that varying the direction of the force α from 0 to 2π by assuming small increments, as in Zibil *et al.*,[33] is not required. In this work α is an unknown variable and is determined analytically. This makes the new approach more computationally efficient and more accurate because the results no longer depend on the precision of the increment used for α.

If the performance index value lies on a vertex of the polytope, all three actuators will be set to their extreme capabilities. Eight possible combinations exist due to the two extreme magnitudes of the torque outputs $\tau_{i_{\min}}$ or $\tau_{i_{\max}}$. If the performance index value lies on an edge of the polytope, two actuators are set to their extreme output capabilities, while the third actuator will be working within its output range and will be referred to as being in transition (τ_t). Torques that are not at their extreme capabilities are said to be in transition because they will transfer from one torque limit to the opposite limit, e.g., from $\tau_{i_{\min}}$ to $\tau_{i_{\max}}$. A torque in transition is an unknown variable in $\mathbf{x}$. Twelve combinations exist for this case, i.e., three combinations of torques at their extreme values (two out of three output torques) and four combinations of the extreme magnitudes ($\tau_{i_{\min}}$ or $\tau_{i_{\max}}$). If the performance index value lies on a facet of the polytope, one actuator is set to an extreme capability and the other two torques will be in transition. Six combinations exist, one out of three torques is set to an extreme magnitude ($\tau_{i_{\min}}$ or $\tau_{i_{\max}}$).

Once all the combinations are evaluated, the performance index can be determined as the maximum f or m_z, as formulated in Eq. (1). If the problem involves finding a torque in transition, it is important to verify that this torque does not exceed its torque output capabilities.

3.2. Maximum force with a prescribed moment ($^{pm}F_{app}$ and $^{pm}F_{iso}$)

This study provides the information of the maximum force that can be applied (or sustained) by the mobile platform for

https://doi.org/10.1017/S0263574708004384 Published online by Cambridge University Press

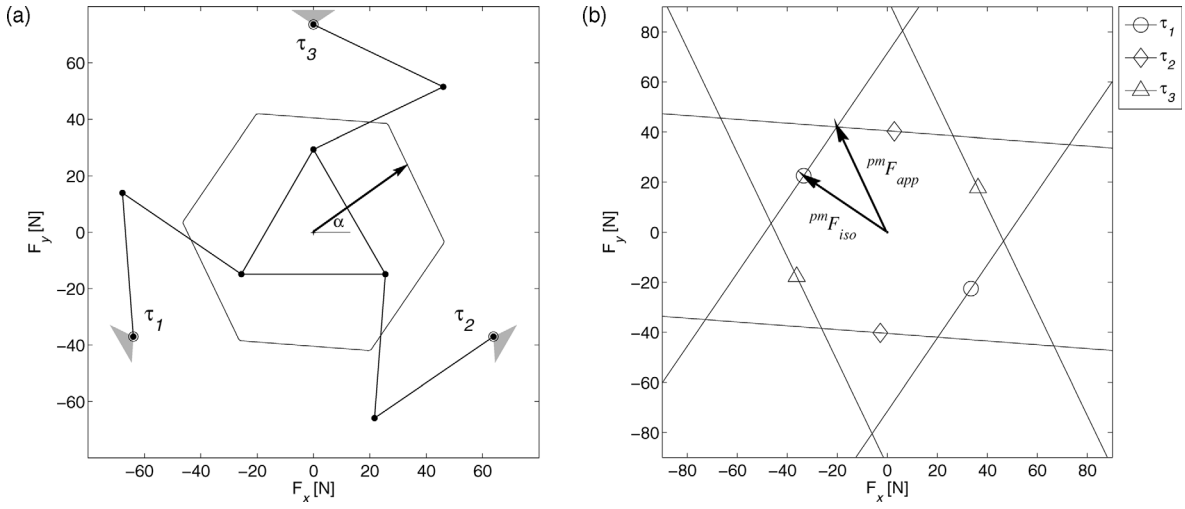

Fig. 2. Generation of a force capability polygon.

a prescribed (specified) moment m_z. Assume the case when $m_z = 0$ yielding a pure force analysis. The force capability of a PPM can be illustrated with a force polygon. The hexagon shown in Fig. 2a illustrates the force polygon. For an arbitrary direction α, the distance from the center of the force space to the polygon is proportional to the magnitude of the force that can be applied or sustained.

The sets of parallel lines in Fig. 2b represent the cross section of the parallel planes that constrain an actuator torque at $m_z = 0$. Since the polytope is centro-symmetric when the extreme magnitudes are equal, the force polygon will show elements of symmetry at $m_z = 0$. The area between these parallel lines represents the force that one actuator can sustain in any direction. The area enclosed by all the lines, a polygon, represents the force capabilities of the system ${}^{pm}F$ for that prescribed moment. When $m_z \neq 0$, the polygon is usually irregular. Figure 2b also shows ${}^{pm}F_{app}$ and ${}^{pm}F_{iso}$, the maximum applicable force and the maximum isotropic force, respectively. Forces ${}^{pm}F_{app}$ and ${}^{pm}F_{iso}$ may be seen as the radii of the circle that encloses the force polygon and the circle that is inscribed in the force polygon, respectively. These forces can be used as performance indices of the manipulator. Finotello *et al.*[25] defined these indices as maximum available value (MAV) and maximum isotropic value (MIV), respectively.

The vertices of the force polygon are generated with the intersection of two lines. Thus, vertices can be found by setting two actuators to their extreme output capabilities. The third actuator will be in transition. Mathematically, Eq. (10) contains five unknown variables, i.e., f_x, f_y, and τ_i for $i = 1, 2, 3$. By assuming two actuator torques to be evaluated at their extreme output capabilities, a fully constrained system results (three variables in three equations). Therefore, Eq. (10) can be rearranged as a linear system of equations of the form $\mathbf{Ax} = \mathbf{b}$, where $\mathbf{x} = [\, f_x \quad f_y \quad \tau_t \,]^{\mathrm{T}}$, i.e.,

$$[\$'\mathbf{D}]\boldsymbol{\tau} = \mathbf{F} \Rightarrow \mathbf{Ax} = \mathbf{b} \tag{12}$$

$$\begin{bmatrix} sd_{1,1} & sd_{1,2} & sd_{1,3} \\ sd_{2,1} & sd_{2,2} & sd_{2,3} \\ sd_{3,1} & sd_{3,2} & sd_{3,3} \end{bmatrix} \begin{bmatrix} \tau_1 \\ \tau_2 \\ \tau_3 \end{bmatrix} = \begin{bmatrix} f_x \\ f_y \\ m_z \end{bmatrix}$$

$$\Rightarrow \underbrace{\begin{bmatrix} 1 & 0 & -sd_{1,t} \\ 0 & 1 & -sd_{2,t} \\ 0 & 0 & -sd_{3,t} \end{bmatrix}}_{A} \underbrace{\begin{bmatrix} f_x \\ f_y \\ \tau_t \end{bmatrix}}_{x}$$

$$= \underbrace{\begin{bmatrix} sd_{1,m_1} & sd_{1,m_2} \\ sd_{2,m_1} & sd_{2,m_2} \\ sd_{3,m_1} & sd_{3,m_2} \end{bmatrix} \begin{bmatrix} \pm\tau_{m_1} \\ \pm\tau_{m_2} \end{bmatrix} - \begin{bmatrix} 0 \\ 0 \\ m_z \end{bmatrix}}_{b}.$$

All possible combinations of torques at their extreme capabilities and their magnitudes are considered. There are twelve combinations in total. All combinations are evaluated and the force polygon is generated by enclosing feasible solutions; i.e., solutions where the torque in transition does not exceed its torque output capabilities. Figure 2b shows twelve intersections: six intersection points occur outside the polygon (one actuator would have to work over its limits) and six intersection points define the vertices of the polygon.

The performance index ${}^{pm}F_{app}$ corresponds to the combination of torques that yields the maximum force f, where $f = \sqrt{f_x^2 + f_y^2}$. While, ${}^{pm}F_{iso}$ is determined by finding the shortest distance between the origin of the force space and the polygon.

Shown in Fig. 3a is the polytope of this manipulator formed by stacking polygons at different m_z. Figure 3b shows the top view of the polyhedron. The dark hexagon in Figs. 3a and 3b illustrates the force polygon at $m_z = 0$. Geometrically, ${}^{pm}F_{app}$ will be a point on an edge of the polytope and ${}^{pm}F_{iso}$ will be a point on a facet of the polytope.

3.3. Maximum reachable force (${}^{mr}F_{app}$ and ${}^{mr}F_{iso}$)

This study provides the information of the maximum forces that can be applied or sustained. The maximum reachable force that can be applied by the manipulator has an associated moment. There are six unknown variables, i.e., f_x, f_y, m_z, and τ_i for $i = 1, 2, 3$, in Eq. (10). Thus all three

https://doi.org/10.1017/S0263574708004384 Published online by Cambridge University Press

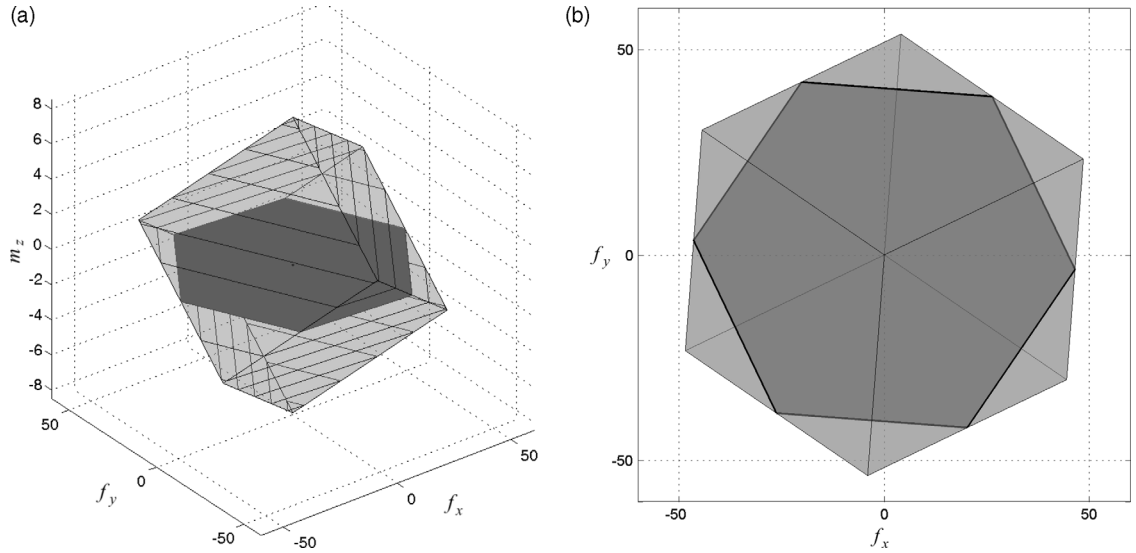

Fig. 3. Wrench polytope and force polygon at $m_z = 0$.

actuator outputs can be set to their extreme capabilities. This yields a linear system of the form $\mathbf{Ax} = \mathbf{b}$, where $\mathbf{x} = [f_x \quad f_y \quad m_z]^T$. Through the linear transformation of Eq. (11), each extreme magnitude combination leads to a vertex of the polytope. A force polygon may be generated by projecting these vertices on the force plane as shown in Fig. 4. This polygon represents the maximum reachable force, ${}^{mr}F$. Performance indices ${}^{mr}F_{iso}$ and ${}^{mr}F_{app}$ can also be determined. Geometrically, ${}^{mr}F_{app}$ will be a vertex of the polytope and ${}^{mr}F_{iso}$ will be a point on an edge of the polytope.

3.4. Maximum moment with a prescribed force (${}^{pf}M_z$)

This study provides the information of the range of m_z that can be used for a completely prescribed force. Since f_x and f_y are known quantities, there are four unknown variables, m_z and τ_i for $i = 1, 2, 3$. Therefore, Eq. (10) will be constrained if one joint torque is at an extreme value. Thus, two actuator outputs will be in transition (τ_{t_a} and τ_{t_b}). This yields a linear system of the form $\mathbf{Ax} = \mathbf{b}$, where $\mathbf{x} = [m_z \quad \tau_{t_a} \quad \tau_{t_b}]^T$. There are six combinations for the 3-RRR PPM to evaluate (the six facets of the polytope) but only two combinations will keep the torques in transition within their actuator capabilities. The larger and smaller solutions represent the upper (${}^{upf}M_z$) and lower (${}^{lpf}M_z$) bound moments, respectively. Figure 5 shows the vector of an arbitrary force. The range of moments can be seen as a vertical line. ${}^{upf}M_z$ and ${}^{lpf}M_z$ are points located on facets of the polytope.

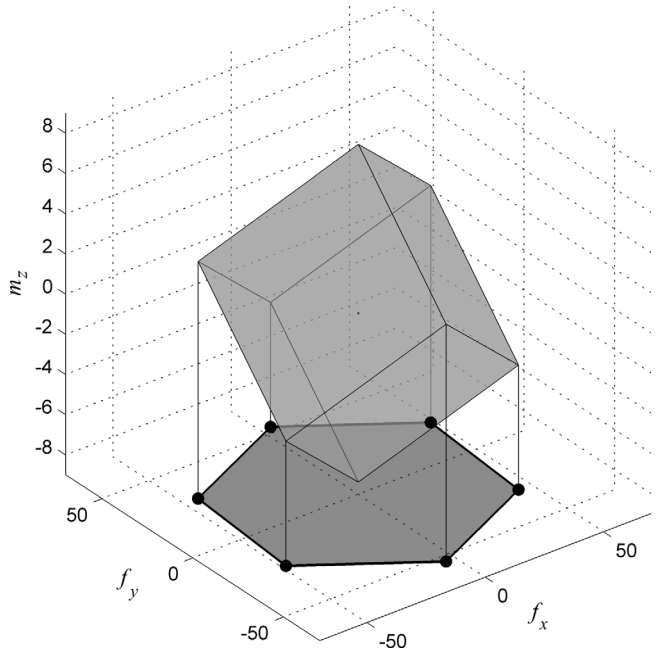

Fig. 4. Wrench polytope and absolute force polygon.

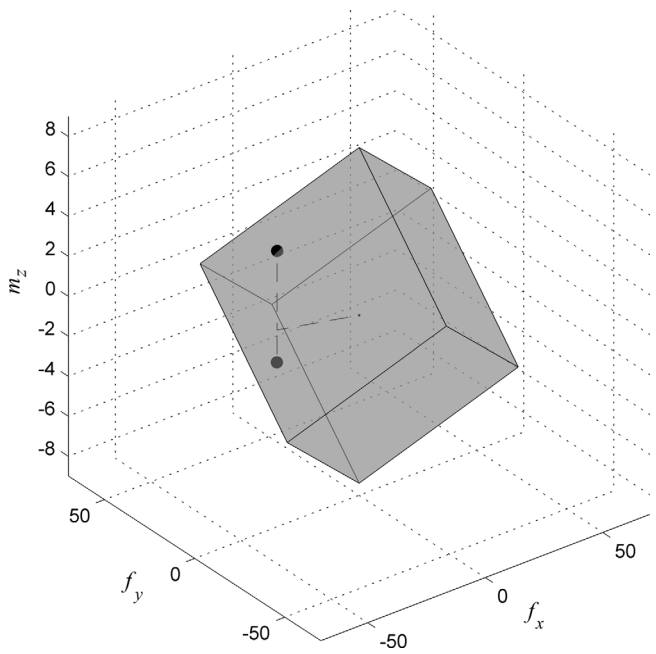

Fig. 5. Maximum moment with a prescribed force.

https://doi.org/10.1017/S0263574708004384 Published online by Cambridge University Press

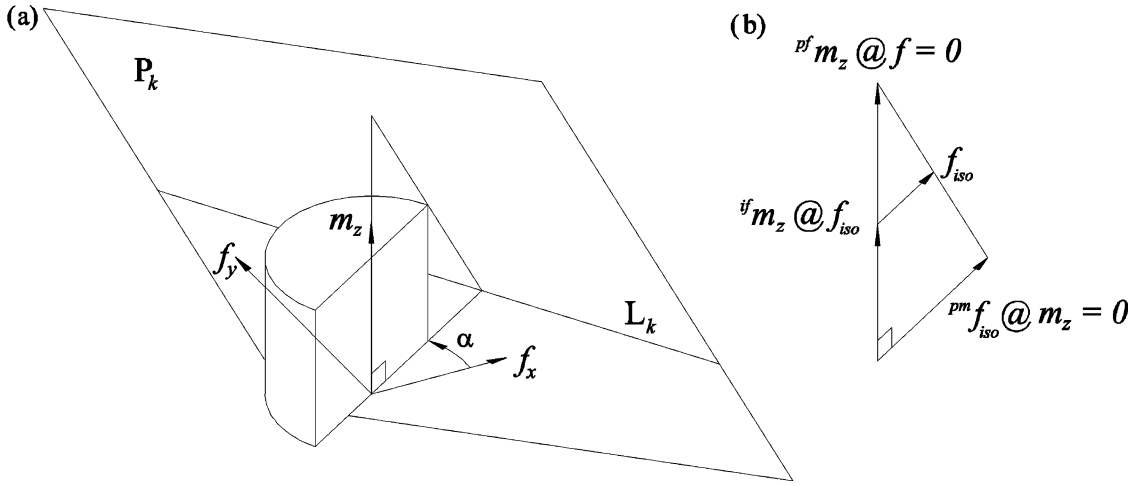

Fig. 6. Similar triangle analysis of the maximum moment with an isotropic force.

3.5. Maximum moment with a prescribed maximum isotropic force (${}^{if}M_z$)

This study provides the information of the range of m_z that can be used for a prescribed maximum isotropic force. This can be seen as the largest cylinder of radius f that can be fully contained within the polytope. This constraint yields another equation; i.e., four in total. There are five unknown variables, m_z, α (direction of the force), and τ_i for $i = 1, 2, 3$. Thus, only one actuator torque can be set to an extreme capability, while two will be in transition. Since two torques will be in transition, the intersection of the isotropic force cylinder with the polytope will occur at one facet of the polytope.

This problem cannot be solved by simply rearranging Eq. (10). As an alternative, a geometrical analysis of the problem is considered. For non-redundant manipulators, the polytope is generated with three sets of parallel planes. The maximum moment with a prescribed isotropic force (${}^{if}M_z$) of the manipulator can be determined by comparing the resulting isotropic moment associated with every plane. Isotropy is ensured with the plane that yields the minimum of the maximum moment, ${}^{if}M_z = \min({}^{if}m_z)$, i.e., the cylinder would be fully inscribed in the polytope. Let the k^{th} plane ($\mathbf{P}_k$) be generated with one of the torques acting at an extreme capability, e.g.,

$$\mathbf{P}_k = \left\{ \left[\$'\mathbf{D}\right]\boldsymbol{\tau} \,|\, \boldsymbol{\tau} = \begin{bmatrix} \tau_{1_{\max}} & \tau_{t_a} & \tau_{t_b} \end{bmatrix}^T, \tau_{2_{\min}} \le \tau_{t_a} \le \tau_{2_{\max}}, \; \tau_{3_{\min}} \le \tau_{t_b} \le \tau_{3_{\max}} \right\} \tag{13}$$

Shown in Fig. 6a is a half-section of the isotropic force cylinder (radius f_{iso}) intersecting $\mathbf{P}_k$. The goal is to determine the height of this cylinder (${}^{if}m_z$).

Let ${}^{pm}f_{iso}$ be the isotropic force at $m_z = 0$. Geometrically, this force represents the radius of a circle tangent to $\mathbf{P}_k$. If the moment is varied, the corresponding isotropic forces will form circles of different radii. The intersection points between each circle and $\mathbf{P}_k$ will form a line as shown in Fig. 6a. When the axis of the cylinder intersects $\mathbf{P}_k$ the magnitude of the force will be zero. As a consequence, a triangle results and ${}^{if}m_z$ can be determined, for any prescribed isotropic force, as a similar triangle problem as illustrated in Fig. 6b. Thus, the problem requires finding the base (${}^{pm}f_{iso}$) and the height (${}^{pf}m_z$) of the triangle.

To find ${}^{pm}f_{iso}$ set $m_z = 0$. The third row of Eq. (10) yields,

$$a_0\tau_{t_a} + a_1\tau_{t_b} + a_2 = 0 \tag{14}$$

where $a_0 = sd_{3,2}$, $a_1 = sd_{3,3}$, and $a_2 = sd_{3,1}\tau_{1_{\max}}$. Solve for τ_{t_b} and substitute it back in the first two rows of Eq. (10). This yields two equations in terms of f_x and f_y, i.e.,

$$b_{11}\tau_{t_a} + b_{12} = f_x \tag{15a}$$

$$b_{21}\tau_{t_a} + b_{22} = f_y \tag{15b}$$

Hence, τ_{t_a} is eliminated yielding,

$$\mathbf{L}_k = c_0 f_x + c_1 f_y + c_2 = 0 \tag{16}$$

This equation describes the line generated by the intersection of $\mathbf{P}_k$ with the plane $m_z = 0$, denoted as $\mathbf{L}_k$. The shortest distance from the origin of the force space to the line is

$${}^{pm}f_{iso} = \frac{|c_2|}{\sqrt{c_0^2 + c_1^2}} \tag{17}$$

The direction of the force ${}^{pm}f_{iso}$, at $m_z = 0$, can be found with Eq. (16), i.e.,

$$\alpha = \tan^{-1}(c_1/c_0) \tag{18}$$

This angle is used to locate the exact intersection of the isotropic cylinder with $\mathbf{P}_k$. The plane of the triangle described in Fig. 6b is perpendicular to the horizontal plane and therefore ${}^{pm}f_{iso}$ will have the same direction at any m_z.

To find ${}^{pf}m_z$ set $f = 0$. With $f = 0$, Eq. (10) yields

$$a_1\tau_{t_a} + b_1\tau_{t_b} + c_1 = 0 \tag{19a}$$

$$a_2\tau_{t_a} + b_2\tau_{t_b} + c_2 = 0 \tag{19b}$$

$$a_3\tau_{t_a} + b_3\tau_{t_b} + c_3 = m_z \tag{19c}$$

https://doi.org/10.1017/S0263574708004384 Published online by Cambridge University Press

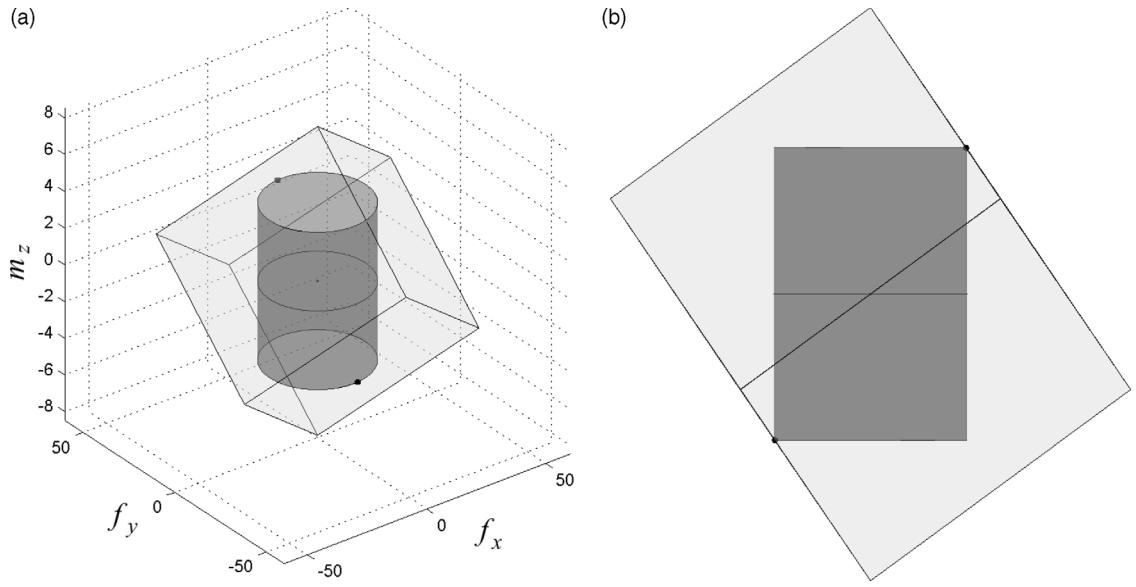

Fig. 7. Maximum moment of a prescribed maximum isotropic force.

where $a_i = sd_{i,2}$, $b_i = sd_{i,3}$, and $c_i = sd_{i,1}\tau_{1_{\max}}$. The first two equations lead to a linear problem and the torques in transition can be found. Substitute τ_{t_a} and τ_{t_b} into the third equation and find ${}^{pf}m_z$ at $f = 0$. Finally, ${}^{if}m_z$ is found using similar triangles.

Repeat the same process with all the planes and find the minimum ${}^{if}m_z$ among all the planes, i.e., ${}^{if}M_z$. Due to the symmetry of the polytope, the same moment will constrain the cylinder in the negative direction. Figure 7a shows an example of ${}^{if}M_z$ for an isotropic force at $f = 20\,\mathrm{N}$. Figure 7a illustrates the isotropic cylinder intersecting the wrench polytope in two points. Figure 7b is a side view of the polytope.

3.6. Maximum moment with a prescribed maximum reachable force (${}^{rf}M_z$)

This study investigates the maximum moment m_z that can be achieved for a prescribed force magnitude. This study can be seen as the intersection of a cylinder of radius f with a point on the polytope which is the farthest away from the $m_z = 0$ plane. Depending on the location of the intersection, different cases must be considered. The intersection can occur either on a facet, on an edge, or on a vertex of the polytope.

Assume the case where the cylinder crosses a plane P_k. The intersection between the cylinder and the plane yields an ellipse, as shown in Fig. 8a. The minimum moment represents the moment associated with an isotropic force as shown in the previous study, whereas the maximum moment ${}^{rf}m_z$ is located at the opposite side of the major axis of the ellipse. Thus, ${}^{rf}m_z$ is determined based on the methodology presented in the previous study. The maximum value of all ${}^{rf}m_z$ yields ${}^{rf}M_z$.

If plane P_k is intersected by another plane, say plane P_j, ${}^{rf}m_z$ is determined with the intersection of the cylinder with a line (or an edge of the polytope), as shown in Fig. 8b. In this case, there are five unknown variables, m_z, α (direction of the force), and τ_i for $i = 1, 2, 3$. Thus, two actuators are set at their extreme values and one will be in transition, i.e.,

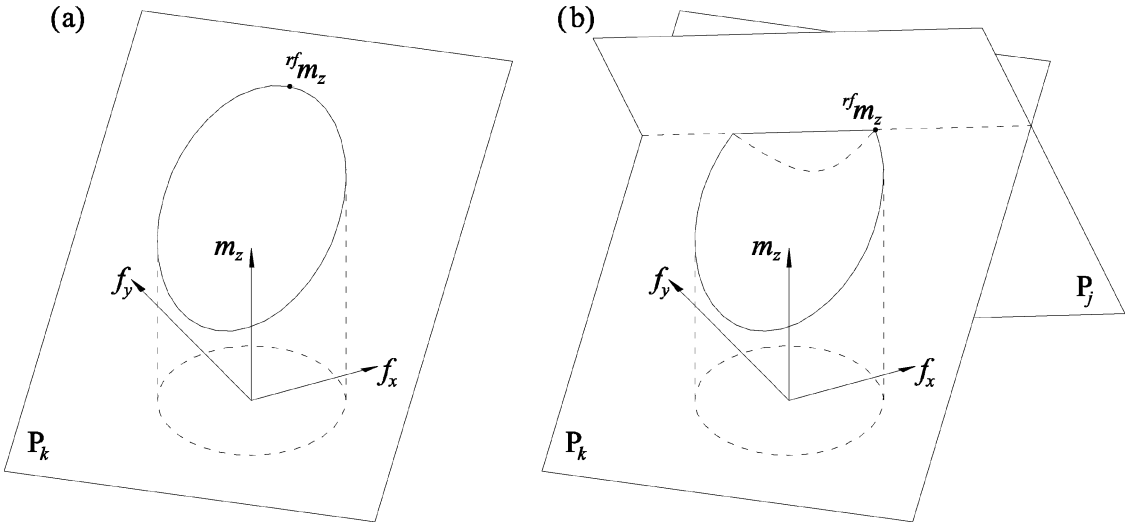

Fig. 8. Intersection of the wrench cylinder with geometrical entities.

https://doi.org/10.1017/S0263574708004384 Published online by Cambridge University Press

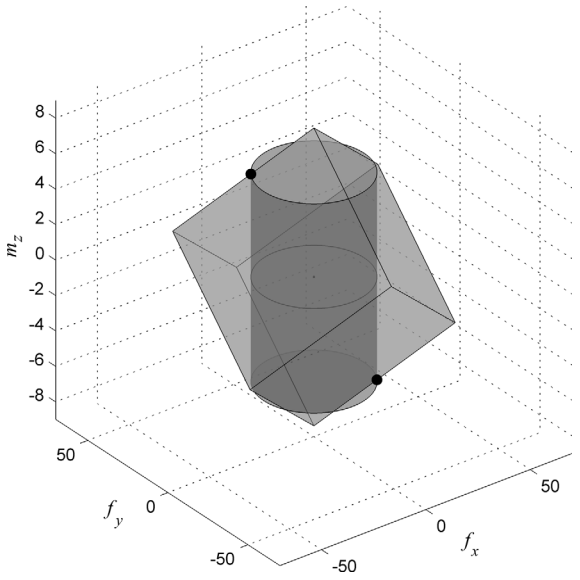

Fig. 9. Maximum moment of a prescribed maximum applicable force.

there are twelve combinations. Given that α is unknown, a non-linear system of equations results with Eq. (10), i.e.,

$$f_x = f\cos(\alpha) = a_{11} + a_{12}\tau_t \tag{20a}$$

$$f_y = f\sin(\alpha) = a_{21} + a_{22}\tau_t \tag{20b}$$

$$m_z = a_{31} + a_{32}\tau_t \tag{20c}$$

where a_{ij} are numerical values.

Eliminate α by squaring and adding Eq. (20a) and Eq. (20b) yielding a quadratic polynomial in τ_t, i.e., there are two intersection points. Find the roots and substitute the larger root that does not exceed its output limits into Eq. (20c). The intersection point where the height of the cylinder is the largest among all feasible solutions yields ${}^{rf}M_z$.

If three planes intersect, ${}^{rf}m_z$ lies on a vertex. This case is unlikely to happen because the vertex must lie on the circle of the cylinder.

Due to the symmetry of the polytope, ${}^{rf}M_z$ can be either positive or negative, as shown in Fig. 9.

3.7. Maximum reachable moment (${}^{mr}M_z$)

This study provides the information of the maximum m_z that can be achieved. The maximum reachable moment has an associated force. In this case, all variables are unknown, i.e., f_x, f_y, m_z, and τ_i for $i = 1, \ldots, 3$. Thus, all actuator outputs can be set to their extreme capabilities yielding an equation of the form

$$sd_{3,1}\left(\tau_{1_{ext}}\right) + sd_{3,2}\left(\tau_{2_{ext}}\right) + sd_{3,3}\left(\tau_{3_{ext}}\right) = m_z \tag{21}$$

The maximum positive moment, ${}^{mr}M_z$, will be obtained by making all the monomials positive. Similarly, the maximum negative moment occurs when all the monomials are negative. Thus, only a single evaluation is required in this study case.

4. Discussion

The proposed performance indices can be also derived for redundantly-actuated PPMs. In Part II of this paper, the authors will analyze the wrench capabilities of revolute-jointed PPMs with additional actuated branches (4-RRR PPM) and in-branch redundancy (3-RRR PPM). In addition, these performance indices will be analyzed throughout their workspace and compared with the non-redundant 3-RRR PPM. Indices associated with the wrench capabilities of the overall workspace will be derived allowing a comparison among these layouts.

5. Conclusion

The wrench capabilities of PPMs are determined by properly adjusting the actuator outputs to their extreme capabilities. This is carried out by mapping the actuator output capabilities from the joint space to the task space. This linear mapping transforms a hypercube into a polytope. The wrench capabilities of the 3-RRR PPM are presented. Six study cases are presented and for each study case performance indices are derived. The evaluation of these performance indices does not require the computationally expensive task of generating graphical polytopes making the performance indices an attractive tool for the design of parallel manipulators.

Acknowledgments

The authors would like to thank the Natural Sciences and Engineering Research Council (NSERC) of Canada for providing financial support for this research.

References

1. Y. F. Zheng and J. Y. S. Luh, "Optimal Load Distribution for Two Industrial Robots Handling a Single Object," *Proceedings of the 1988 IEEE International Conference on Robotics and Automation*, Philadelphia, PA, USA (Apr. 24–29, 1988) pp. 344–349.
2. V. Kumar and K. J. Waldron, "Force Distribution in Closed Kinematic Chains," *Proceedings of the 1988 IEEE International Conference on Robotics and Automation*, Philadelphia, PA, USA (Apr. 24–29, 1988) pp. 114–119.
3. J. M. Tao and J. Y. S. Luh, "Coordination of Two Redundant Manipulators," *Proceedings of the 1989 IEEE International Conference on Robotics and Automation*, Scottsdale, AZ, USA (May 14–19, 1989) pp. 425–430.
4. M. A. Nahon and J. Angeles, "Real-time force optimization in parallel kinematic chains under inequality constraints," *IEEE Trans. Robot. Autom.* **8**(4), 439–450 (1992).
5. W. Kwon and B. H. Lee, "A new optimal force distribution scheme of multiple cooperating robots using dual method," *J. Intell. Robot. Syst.* **21**(4), 301–326 (1998).
6. P. Buttolo and B. Hannaford, "Advantages of Actuation Redundancy for the Design of Haptic Displays," *Proceedings of the 1995 ASME International Mechanical Engineering Congress and Exposition—Part 2*, San Francisco, CA, USA (Nov. 12–17, 1995) pp. 623–630.
7. S. B. Nokleby, R. Fisher, R. P. Podhorodeski and F. Firmani, "Force capabilities of redundantly-actuated parallel manipulators," *Mech. Mach. Theory* **40**(5), 578–599 (2005).
8. V. Garg, J. A. Carretero and S. B. Nokleby, "Determining the Force and Moment Workspace Volumes of Redundantly-Actuated Spatial Parallel Manipulators," *Proeedings of the 2007 ASME Design Engineering Technical Conference ASME*, Las Vegas, NV, USA (Sep. 4–7, 2007).
9. T. Yoshikawa, "Manipulability of robotic mechanisms," *Int. J. Robot. Res.* **4**(2), 3–9 (1985).

https://doi.org/10.1017/S0263574708004384 Published online by Cambridge University Press

10. T. Yoshikawa, *Foundations of Robotics: Analysis and Control* (The MIT Press, Cambridge, MA, USA, 1990).
11. P. Chiacchio, S. Chiaverini, L. Sciavicco and B. Siciliano, "Global task space manipulability ellipsoids for multiple-arm systems," *IEEE Trans. Robot. Autom.* **7**(5), 678–685 (1991).
12. S. Lee and S. Kim, "A Self-Reconfigurable Dual-Arm System," *Proceedings of the1991 IEEE International Conference on Robotics and Automation*, vol. 1, Sacramento, CA, USA, (Apr. 9–11, 1991) pp. 164–169.
13. P. Chiacchio, Y. Bouffard-Vercelli and F. Pierrot, "Evaluation of Force Capabilities for Redundant Manipulators," *Proceedings of the 1996 IEEE International Conference on Robotics and Automation*, vol. 4, Minneeapolis, MN (Apr. 22–28, 1996) pp. 3520–3525.
14. P. Chiacchio, Y. Bouffard-Vercelli and F. Pierrot, "Force polytope and force ellipsoid for redundant manipulators," *J. Robot. Syst.* **14**(8), 613–620 (1997).
15. T. Yoshikawa, "Dynamic manipulability of robot manipulators," *J. Robot. Syst.* **2**(1), 113–124 (1985).
16. P. Chiacchio, "A new dynamic manipulability ellipsoid for redundant manipulators," *Robotica*, **18**(4), 381–387 (2000).
17. J. Duffy, "The fallacy of modern hybrid control theory that is based on 'orthogonal complements' of twist and wrench spaces," *J. Robot. Syst.* **7**(2), 139–144 (1990).
18. K. L. Doty, C. Melchiorri, E. M. Schwartz and C. Bonivento, "Robot manipulability," *IEEE Trans. Robot. Autom.* **11**(3), 462–468 (1995).
19. C. Melchiorri, "Comments on "Global task space manipulability ellipsoids for multiple-arm systems" and further considerations," *IEEE Trans. Robot. Autom.* **9**(2), 232–235 (1993).
20. A. Bicchi, C. Melchiorri and D. Balluchi, "On the mobility and manipulability of general multiple limb robotic systems," *IEEE Trans. Robot. Autom.* **11**(2), 215–228 (1995).
21. A. Bicchi, D. Prattichizzo and C. Melchiorri, "Force and Dynamic Manipulability for Cooperating Robot Systems," *Proceedings of 1997 IEEE/RSJ International Conference on Intelligent Robots and Systems*, vol. 3, Grenoble, France (Sep. 7–11, 1997) pp. 1479–1484.
22. T. Kokkinis and B. Paden, "Kinetostatic Performance Limits of Cooperating Robot Manipulators Using Force-Velocity Polytopes," *Proceedings of the ASME Winter Annual Meeting*, San Francisco, CA, USA (1989) pp. 151–155.
23. J. Lee, " A Study on the Manipulability Measures for Robot Manipulators," *Proceedings of 1997 IEEE/RSJ International Conference on Intelligent Robots and Systems*, vol. 3, Grenoble, France (Sep. 7–11, 1997) pp. 1458–1465.
24. Y. S. Hwang, J. Lee and T. C. Hsia, "A Recursive Dimension-Growing Method for Computing Robotic Manipulability Polytope," *Proceedings of the 2000 IEEE International Conference on Robotics and Automation*, vol. 3, San Francisco, CA, USA (Apr. 24–28, 2000) pp. 2569–2574.
25. R. Finotello, T. Grasso, G. Rossi and A. Terribile, "Computation of Kinetostatic Performances of Robot Manipulators with Polytopes," *Proceedings of the 1998 IEEE International Conference on Robotics and Automation*, vol. 4, Leuven, Belgium (May 16–20, 1998) pp. 3241–3246.
26. P. Gallina, G. Rosati and A. Rossi, "3-d.o.f. wire driven planar haptic interface," *J. Intell. Robot. Syst.* **32**(1), 23–36 (2001).
27. J. Lee and H. Shim, "On the Dynamic Manipulability of Cooperating Multiple Arm Robot Systems," *Proceedings of 2004 IEEE/RSJ International Conference on Intelligent Robots and Systems*, vol. 2, Sendai, Japan (Sep. 28–Oct. 2, 2004) pp. 3520–3525.
28. S. Krut, O. Company and F. Pierrot, "Velocity performance indices for parallel mechanisms with actuation redundancy," *Robotica* **22**(2), 129–139 (2004).
29. S. Krut, O. Company and F. Pierrot, "Force Performance Indexes for Parallel Mechanisms with Actuation Redundancy, Especially for Parallel Wire-Driven Manipulators," *Proceedings of 2004 IEEE/RSJ International Conference on Intelligent Robots and Systems*, vol. 4, Sendai, Japan (Sep. 28–Oct. 2, 2004) pp. 3936–3941.
30. R. T. Rockafellar, *Convex Analysis*, 1st ed. 1970 (Princeton University Press, Princeton, NJ, USA, 1997).
31. V. Visvanathan and L. S. Milor, "An Efficient Algorithm to Determine the Image of a Parallelepiped Under a Linear Transformation," *Proceedings of the Second Annual Symposium on Computational Geometry*, Yorktown Heights, NY, USA, (1986) pp. 207–215.
32. D. R. Chand and S. S. Kapur, "An algorithm for convex polytopes," *J. Assoc. Compu. Mach.* **17**(1), 78–86 (1970).
33. A. Zibil, F. Firmani, S. B. Nokleby and R. P. Podhorodeski, "An explicit method for determining the force-moment capabilities of redundantly-actuated planar parallel manipulators," *Trans. ASME, J. Mech. Des.* **129**(10) 1046–1055 (2007).
34. K. H. Hunt, *Kinematic Geometry of Mechanisms* (Oxford University Press, Toronto, ON, Canada, 1978).
35. R. S. Ball, *A Treatise of the Theory of Screws* (Cambridge University Press, New York, NY, USA, 1900).
36. D. Zlatanov, R. G. Fenton and B. Benhabib, "Analysis of the Instantaneous Kinematics and Singular Configurations of Hybrid-Chain Manipulators," *Proceedings of the ASME 23rd Biennial Mechanisms Conference*, vol. 72, Minneapolis, MN, USA (Sep. 11–14, 1994) pp. 467–476.
37. C. M. Gosselin and J. Angeles, "Singularity analysis of closed-loop kinematic chains," *IEEE Trans. Robot. Autom.* **6**(3), 281–290 (1990).
38. R. Fisher, R. P. Podhorodeski and S. B. Nokleby, "A Reconfigurable Planar Parallel Manipulator," *J. Robot. Syst.* **21**(12), 665–675 (2004).

A. Appendices: A Force Analysis

A screw ($) is a line in space having an associated pitch. A screw quantity can be represented with the Plücker coordinates of a line summed with a term related to the screw direction multiplied by the pitch of the screw.[34] The angular velocity $\boldsymbol{\omega}$ and the translational velocity $\mathbf{v}$ of a point of a moving body may be represented by three-dimensional vectors that can be assembled into a screw quantity $\mathbf{V}$ called an instantaneous twist, $\mathbf{V} = \{\boldsymbol{\omega}^T; \mathbf{v}^T\}^T$.[35] The pitch of the twist is the ratio of the translational velocity to the angular velocity. The pitch of a twist is zero if there is pure rotational velocity about the screw axis, while the pitch of the twist is infinite if there is pure translational velocity along the screw axis.

On the other hand, the resultant force $\mathbf{f}$ and the moment $\mathbf{m}$ acting at a point on the body can be assembled into a similar screw quantity $\mathbf{F}$ called a wrench, $\mathbf{F} = \{\mathbf{f}^T; \mathbf{m}^T\}^T$.[35] The pitch of a wrench is the ratio of the moment to the force. A pure force is a wrench of zero pitch and a pure moment is a wrench of infinite pitch.

In general, the twist and the wrench are composed of six elements, i.e., for a twist, there are three instantaneous rotations about and three instantaneous translations along the axes of a reference frame; while for a wrench there are three pure forces along and three moments about the axes of a reference frame. For a manipulator with $n - DOF$, where $n < 6$, such as planar manipulators, the same $6 - n$ coordinates of the joint twists and the output twist will be zero at any configuration.[36] For planar manipulators, the screw system of planar velocity can be spanned by a rotation and two translations. Therefore, the twist and the wrench will have only three non-zero coordinates. The twist is based on one angular velocity ω_z and two linear velocities v_x and v_y, i.e., $\mathbf{V} = \{\boldsymbol{\omega}^{\mathrm{T}}; \mathbf{v}^{\mathrm{T}}\}^{\mathrm{T}} = \{\omega_z; v_x, v_y\}^{\mathrm{T}}$. While the wrench is comprised of two forces f_x and f_y and one moment m_z, i.e., $\mathbf{F} = \{\mathbf{f}^{\mathrm{T}}; \mathbf{m}^{\mathrm{T}}\}^{\mathrm{T}} = \{f_x, f_y; m_z\}^{\mathrm{T}}$. Another way to express the

https://doi.org/10.1017/S0263574708004384 Published online by Cambridge University Press

wrench is $\mathbf{F} = \{f\cos\alpha,\ f\sin\alpha; m_z\}^{\mathrm{T}}$, where f and α are the magnitude and direction of the force, respectively.

The forces that can be applied (sustained) by a branch can be modelled with associated reciprocal screws.[36] The force exerted by the k^{th} actuated joint of the i^{th} branch is characterized by a screw, $\$'_{k_i} = \{(\$'_{k_i})_z; (\$o'_{k_i})_x, (\$o'_{k_i})_y\}^{\mathrm{T}}$, reciprocal to all joints of the i^{th} branch except for the actuated joint k, i.e.,

$$\$_{j_i} \circledast \$'_{k_i} = (\$_{j_i})_x (\$o'_{k_i})_x + (\$_{j_i})_y (\$o'_{k_i})_y + (\$o_{j_i})_z (\$'_{k_i})_z = 0, \text{ for } j \neq k \qquad (22)$$

where $\$_{j_i} = \{(\$_{j_i})_x, (\$_{j_i})_y; (\$o_{j_i})_z\}^{\mathrm{T}}$ denotes the screw coordinates of all joints $j \neq k$ of the i^{th} branch and $\circledast$ denotes the reciprocal product between two screws.

The wrench applied by a parallel manipulator is the sum of wrenches applied by all m actuated joints of the manipulator. In matrix form, the static force solution is:

$$\mathbf{F}_{3\times 1} = [\$']_{3\times m}\mathbf{w}_{m\times 1} \qquad (23)$$

where $[\$']$ is referred to as the associated reciprocal screw matrix and $\mathbf{w}$ the vector of wrench intensities. The torque applied by the k^{th} actuated joint of the i^{th} branch is

$$\tau_{k_i} = w_{k_i}(\$_{k_i} \circledast \$'_{k_i}) \qquad (24)$$

Therefore, the wrench intensity is

$$w_{k_i} = \frac{\tau_{k_i}}{(\$_{k_i} \circledast \$'_{k_i})} \qquad (25)$$

The relationship among all the wrench intensities in the system yields:

$$\mathbf{w} = [\mathbf{D}]\boldsymbol{\tau} \qquad (26)$$

where $[\mathbf{D}]$ is a diagonal matrix whose entries are $1/(\$_{k_i} \circledast \$'_{k_i})$.

Combining Eq. (26) with Eq. (23) results in the forward static force solution, i.e.,

$$[\$'\mathbf{D}]_{3\times m}\boldsymbol{\tau}_{m\times 1} = \mathbf{F}_{3\times 1} \qquad (27)$$

where $[\$'\mathbf{D}] = [\$'][\mathbf{D}]$.

An alternative formulation of the static force analysis is obtained by differentiating the loop-closure equations which involve the input $\mathbf{q}$ (joint displacements) and output $\mathbf{x}$ (position and orientation) of the end-effector with respect to time.

Gosselin and Angeles[37] presented the relationship between the input $\dot{\mathbf{q}}$ (joint rates) and output $\dot{\mathbf{x}}$ (end-effector's velocity) speeds as:

$$[\mathbf{A}]_{3\times m}\,\dot{\mathbf{x}}_{3\times 1} = [\mathbf{B}]_{m\times m}\,\dot{\mathbf{q}}_{m\times 1} \qquad (28)$$

where

$$[\mathbf{A}] = \frac{\partial f(\mathbf{q}, \mathbf{x})}{\partial \mathbf{x}} \quad \text{and} \quad [\mathbf{B}] = \frac{\partial f(\mathbf{q}, \mathbf{x})}{\partial \mathbf{q}}$$

This leads to the inverse velocity problem, i.e.,

$$\dot{\mathbf{q}} = [\mathbf{J}]^{-1}\,\dot{\mathbf{x}} \qquad (29)$$

where $[\mathbf{J}]^{-1} = [\mathbf{B}]^{-1}[\mathbf{A}]$.

Under static conditions the conservation of power relationship is defined as:

$$P_{in} = P_{out}$$
$$\boldsymbol{\tau}^{\mathrm{T}}\dot{\mathbf{q}} = \mathbf{F}^{\mathrm{T}}\dot{\mathbf{x}} \qquad (30)$$

By combining Eq. (30) with Eq. (29) the following static force relationship results:

$$[\mathbf{J}]^{-\mathrm{T}}_{3\times m}\boldsymbol{\tau}_{m\times 1} = \mathbf{F}_{3\times 1} \qquad (31)$$

where $\boldsymbol{\tau}$ is referred to as the vector of articular forces (torques or forces) and $\mathbf{F}$ is referred to as the vector of generalized forces (wrenches).

Notice that both formulations are equivalent, i.e., $[\$'\mathbf{D}]_{3\times m} = [\mathbf{J}]^{-\mathrm{T}}_{3\times m}$.

B. Description of the Manipulator

The dimensions and the actuator capabilities of the 3-RRR PPM are modelled after the Reconfigurable Planar Parallel Manipulator (RPPM) designed by Fisher *et al.*[38] This manipulator is comprised of two platforms (base and mobile) that are connected by three branches, as shown in Fig. 10. The base and the mobile platforms of the RPPM are equilateral triangles. The base and mobile platform edge lengths are 0.5 m and 0.2 m, respectively. Each branch contains two links and three revolute joints. The lengths of the first and second links of each branch are 0.2 m. The first joints are actuated (solid circles), while the second and third joints are passive joints (empty circles). The extreme output torque capabilities of the actuators (based on the existing actuators of the RPPM) are ±4.2 Nm.

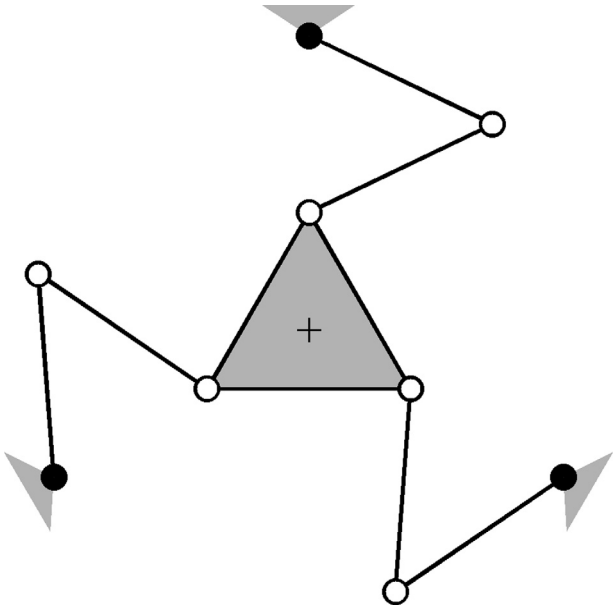

Fig. 10. 3-RRR planar parallel manipulator.

https://doi.org/10.1017/S0263574708004384 Published online by Cambridge University Press